Stress Analyses of Laminated Thick-Walled Cylindrical Anisotropic Shells

O-Il Byon*
College of Industrial Technology, Nihon University, Chiba 285, Japan
and
Jack R. Vinson†
University of Delaware, Newark, Delaware 19716

A simple and accurate finite cylindrical element method is formulated for obtaining stresses and deformations in laminated thick-walled cylindrical anisotropic shells. This method effectively reduces the three-dimensional problem to a one-dimensional problem. The method is illustrated by the study of a thick-walled cylindrical shell composed of graphite/epoxy, with a $(90°_5/0°_5/90°_5)_8$ stacking sequence, subjected to an external uniform pressure. It is found that significant tensile radial strains occur near the inner surface, which can cause a failure of the shell. It is also found that these tensile strains are functions of the Poisson's ratios of the composite material. Therefore, in design, choosing materials with smaller Poisson's ratios alleviates this problem.

Nomenclature

a	= inner radius
$[B]$, $[B_{mn}]$	= strain matrices
C_m, C_n	= quantities defined in Eq. (3)
$\{d\}$	= displacement vector
E_{11}, E_{22}, E_{33}	= elastic moduli
$\{F\}_p$	= nodal force vector
G_{12}, G_{13}, G_{23}	= shear moduli
h	= thickness of cylindrical shell
i, $i+1$	= nodal surfaces
$[K]$, $[K_{mn}]$	= stiffness matrices
m,n	= wave numbers in Fourier series
$[N_d]$,$[N_{dmn}]$	= shape function matrices
$[N_p]$,$[N_{pmn}]$	= surface loads matrices
p_i, p_o	= internal and external pressures
$\{p_0\}$	= uniform surface loads vector
p_{x0}, p_{y0}, p_{z0}	= components of $\{p_0\}$
$\{p\}$	= vector defined in Eq.(1)
p_x, p_y, p_z	= components of $\{p\}$
$[\bar{Q}]$	= elasticity matrix
R	= mean radius, $a + h/2$
r	= last wave number of Fourier series
S_m, S_n	= quantities defined in Eq.(3)
u, v, w	= displacements in the x, y, z direction
V	= potential energy
x, $y(\theta)$, z	= cylindrical coordinates
$\{\delta\}$, $\{\delta_{mn}\}$	= nodal displacement vectors
$\{\epsilon\}$	= strain tensor
ϵ_x, ϵ_y, ϵ_z	= normal strains
γ_{xy}, γ_{xz}, γ_{yz}	= shearing strains
ν_{12}, ν_{13}, ν_{23}	= Poisson's ratios
$\{\sigma\}$	= stress tensor
σ_x, σ_y, σ_z	= normal stresses
τ_{xy}, τ_{xz}, τ_{yz}	= shearing stresses

Received March 19, 1990; presented as Paper 90-0921 at the AIAA/ASME/ASCE/AHS/ASC 31st Structures, Structural Dynamics, and Materials Conference, Long Beach, CA, April 2-4, 1990; revision received Aug. 28, 1990; accepted for publication Aug. 28, 1990.

*(or Goichi Ben) Professor, Department of Mechanical Engineering, 1-2-1, Izumicho, Narashino. Member AIAA.

†H. Fletcher Brown Professor of Mechanical and Aerospace Engineering, Associate Fellow AIAA.

Introduction

THE design of a composite material pressure vessel is currently being considered for deep submergence research vehicle applications. To implement such a design, a thick laminate must be incorporated because of the high external hydrostatic pressure. In general, the present state of the art for design of thick-walled shells involves methods based either upon the plane strain assumption, thin-walled shell theory, or a three-dimensional finite element method.

Several texts (e.g., Comings[1]) have dealt with thick-walled pressure vessels, but have provided only Lamé's plane strain solution for determining stresses and wall thickness. Vinson[2] developed an analytical method for a shell with ratios of wall thickness to mean radius as large as 0.5 and gave the accurate explicit solution by use of elasticity solutions and Legendre polynomials, or closely related functions. However, his method was restricted to isotropic shells. Hyer[3] analyzed a cross-ply graphite/epoxy cylinder with ratios of wall thickness to mean radius of 0.1 and 0.2 subjected to an external hydrostatic pressure. His analysis was based on a generalized plane deformation elasticity solution. He and his coauthors[4,5] also presented solutions accounting for thermal stresses and deformations in composite tubes. Peros[6] showed that a large Poisson's ratio caused significant tensile radial strains in the graphite/epoxy cylindrical shells under an external pressure, resulting from hoop and axial compressive stresses. However, his "smeared" analysis was at variance with his experimental data. Furthermore, Vanderpool and Bert[7] analyzed the resonant vibration frequencies of a fiber-reinforced, thick-walled, circular cylindrical shell of finite length.

Methods of analysis are developed herein for a very thick-walled cylindrical anisotropic shell under external and/or internal pressures. The present theory does not employ any shell theory assumptions, but uses the one-dimensional finite element method. This requires a thick-walled cylindrical shell to be divided into a number of thin cylindrical elements in the through-the-thickness direction. Although a linear polynomial is used in the finite element method in the radial direction, orthogonal function series are used in the axial and circumferential directions. As a result, the assembled stiffness matrix

size for the thick-walled cylindrical shell is relatively small since this shell has subdivisions only in the through-the-thickness direction and no subdivisions in the axial and the circumferential directions.

Analysis

An anisotropic thick-walled cylindrical shell having an inner radius, length, and thickness of a, L, and h, respectively, is illustrated in Fig. 1. The origin of cylindrical coordinates is located at any point on the inner radius surface and the cylindrical shell is divided only into the radial direction with an element that has a cylindrical shell shape, and is shown by the hatched area in Fig. 1. When the cylindrical shell is simply supported at both ends and is subjected to uniform surface loads p_{x0}, p_{y0}, and p_{z0} over the entire surface of cylindrical shell, these surface loads are resolved into Fourier series as follows:

$$\{p\} = \begin{Bmatrix} p_x \\ p_y \\ p_z \end{Bmatrix} = \begin{Bmatrix} \sum_m^r \sum_n^r \frac{4p_{x0}}{mn\pi^2}(1-\cos m\pi)(1-\cos n\pi)C_mS_n \\ \sum_m^r \sum_n^r \frac{4p_{y0}}{mn\pi^2}(1-\cos m\pi)(1-\cos n\pi)S_mC_n \\ \sum_m^r \sum_n^r \frac{4p_{z0}}{mn\pi^2}(1-\cos m\pi)(1-\cos n\pi)S_mS_n \end{Bmatrix} \tag{1}$$

and can be rewritten in matrix form

$$\{p\} = \sum_m^r \sum_n^r [N_{pmn}]\{p_{0mn}\} = [N_p]\{p_0\} \tag{2}$$

where

$$C_m = \cos(m\pi x/L), \qquad C_n = \cos(n\theta/2)$$
$$S_m = \sin(m\pi x/L), \qquad S_n = \sin(n\theta/2) \tag{3a}$$

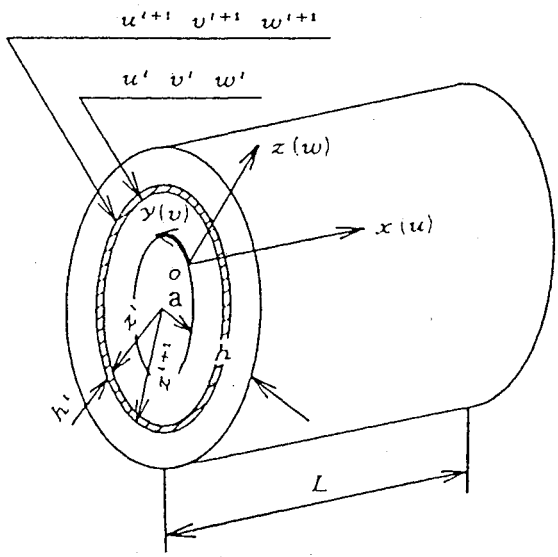

Fig. 1 Coordinate system and displacement parameters for the finite cylindrical element formulation.

$$[N_{pmn}] = \begin{bmatrix} C_mS_n & 0 & 0 \\ 0 & S_mC_n & \\ 0 & 0 & S_mS_n \end{bmatrix} \tag{3b}$$

$$\{p_{0mn}\} = \frac{4(1-\cos m\pi)(1-\cos n\pi)}{mn\pi^2} \begin{Bmatrix} p_{x0} \\ p_{y0} \\ p_{z0} \end{Bmatrix} \tag{3c}$$

$$[N_p] = \{[N_{p11}], [N_{p31}], \ldots, [N_{pr1}], \ldots, [N_{pmn}], \ldots, [N_{prr}]\} \tag{3d}$$

$$\{p_0\}^T = [\{p_{011}\}^T, \{p_{031}\}^T, \ldots, \{p_{0r1}\}^T, \ldots, \times \{p_{0mn}\}^T, \ldots, \{p_{0rr}\}^T] \tag{3e}$$

In these equations, m and n have to be taken as odd numbers, and the last number r is considered the same value in all the series. If u^i_{mn}, v^i_{mn}, w^i_{mn}, u^{i+1}_{mn}, v^{i+1}_{mn}, and w^{i+1}_{mn} are the displacement parameters for a typical cylindrical element with nodal surface i and $i+1$, the displacement functions u, v, and w for this cylindrical element are defined as

$$\{d\} = \begin{Bmatrix} u \\ v \\ w \end{Bmatrix} = \sum_m^r \sum_n^r [N_{dmn}]\{\delta_{mn}\} = [N_d]\{\delta\} \tag{4}$$

where

$$[N_{dmn}] = \begin{bmatrix} C_mS_nf^i & 0 & 0 & C_mS_nf^{i+1} & 0 & 0 \\ 0 & S_mC_nf^i & 0 & 0 & S_mC_nf^{i+1} & 0 \\ 0 & 0 & S_mS_nf^i & 0 & 0 & S_mS_nf^{i+1} \end{bmatrix} \tag{5a}$$

$$\{\delta_{mn}\}^T = \{u^i_{mn}, v^i_{mn}, w^i_{mn}, u^{i+1}_{mn}, v^{i+1}_{mn}, w^{i+1}_{mn}\} \tag{5b}$$

$$[N_d] = \{[N_{d11}], [N_{d31}], \ldots, [N_{dr1}], \ldots, [N_{dmn}], \ldots, [N_{drr}]\} \tag{5c}$$

$$\{\delta\}^T = [\{\delta_{11}\}^T, \{\delta_{31}\}^T, \ldots, \{\delta_{r1}\}^T, \ldots, \{\delta_{mn}\}^T, \ldots, \{\delta_{rr}\}^T] \tag{5d}$$

$$f^i = (z^{i+1}-z)/(z^{i+1}-z^i), \quad f^{i+1} = (z-z^i)/(z^{i+1}-z^i) \tag{5e}$$

Each layer is assumed to be a monoclinic linear elastic material. The constitutive equations for a lamina of a fiber reinforced composite material in terms of the $x-y(\theta)-z$ coordinate system are given as

$$\begin{Bmatrix} \sigma_x \\ \sigma_y \\ \sigma_z \\ \tau_{yz} \\ \tau_{zx} \\ \tau_{xy} \end{Bmatrix} = \begin{bmatrix} \bar{Q}_{11} & \bar{Q}_{12} & \bar{Q}_{13} & 0 & 0 & \bar{Q}_{16} \\ \bar{Q}_{12} & \bar{Q}_{22} & \bar{Q}_{23} & 0 & 0 & \bar{Q}_{26} \\ \bar{Q}_{13} & \bar{Q}_{23} & \bar{Q}_{33} & 0 & 0 & \bar{Q}_{36} \\ 0 & 0 & 0 & \bar{Q}_{44} & \bar{Q}_{45} & 0 \\ 0 & 0 & 0 & \bar{Q}_{45} & \bar{Q}_{55} & 0 \\ \bar{Q}_{16} & \bar{Q}_{26} & \bar{Q}_{36} & 0 & 0 & \bar{Q}_{66} \end{bmatrix} \begin{Bmatrix} \epsilon_x \\ \epsilon_y \\ \epsilon_z \\ \gamma_{yz} \\ \gamma_{zx} \\ \gamma_{xy} \end{Bmatrix} \tag{6a}$$

or

$$\{\sigma\} = [\bar{Q}]\{\epsilon\} \tag{6b}$$

The strain-displacement relations for any elastic body expressed in cylindrical coordinates are given as

$$\epsilon_x = \frac{\partial u}{\partial x}, \qquad \epsilon_y = \frac{\partial v}{(a+z)\partial\theta} + \frac{w}{(a+z)} \tag{7a}$$

$$\epsilon_z = \frac{\partial w}{\partial z}, \qquad \gamma_{zv} = \frac{\partial v}{\partial z} + \frac{\partial w}{(a+z)\partial\theta} - \frac{v}{(a+z)} \tag{7b}$$

$$\gamma_{zx} = \frac{\partial w}{\partial x} + \frac{\partial u}{\partial z}, \qquad \gamma_{xy} = \frac{\partial u}{(a+z)\partial\theta} + \frac{\partial v}{\partial x} \tag{7c}$$

Substituting Eq. (4) into Eqs. (7) results in

$$\{\epsilon\} = \sum_m^r \sum_n^r [B_{mn}]\{\delta_{mn}\} = [B]\{\delta\} \tag{8}$$

where

$$[B_{mn}] = \begin{bmatrix} \frac{-m\pi}{L} S_m S_n f^i & 0 & 0 \\ 0 & -\frac{nf^i S_m S_n}{2(a+z)} & \frac{S_m S_n f^i}{a+z} \\ 0 & 0 & \frac{-S_m S_n}{z^{i+1}-z^i} \\ 0 & -\frac{S_m C_n}{Z^{i+1}-Z^i} - \frac{f^i S_m C_n}{a+z} & \frac{nf^i S_m C_n}{2(a+z)} \\ \frac{-C_m S_n}{z^{i+1}-z^i} & 0 & \frac{m\pi}{L} C_m S_n f^i \\ \frac{nf^i C_m C_n}{2(a+z)} & \frac{m\pi}{L} C_m C_n f^i & 0 \end{bmatrix}$$

$$\begin{bmatrix} \frac{-m\pi}{L} S_m S_n f^{i+1} & 0 & 0 \\ 0 & -\frac{nf^{i+1} S_m S_n}{2(a+z)} & \frac{S_m S_n f^{i+1}}{a+z} \\ 0 & 0 & \frac{S_m S_n}{z^{i+1}-z^i} \\ 0 & \frac{S_m C_n}{Z^{i+1}-Z^i} - \frac{f^{i+1} S_m C_n}{a+z} & \frac{nf^{i+1} S_m C_n}{2(a+z)} \\ \frac{C_m C_n}{z^{i+1}-z^i} & 0 & \frac{m\pi f^{i+1}}{L} C_m S_n \\ \frac{nf^{i+1} C_m C_n}{2(a+z)} & \frac{m\pi}{L} C_m C_n f^{i+1} & 0 \end{bmatrix}$$

$$[B] = \{[B_{11}], [B_{31}], \ldots, [B_{r1}], \ldots, [B_{mn}], \ldots, [B_{rr}]\} \tag{9}$$

The potential energy V neglecting the body forces can be given as

$$V = \frac{1}{2}\int_v \{\epsilon\}^T\{\sigma\}\, dv - \int_s \{d\}^T\{p\}\, ds \tag{10}$$

Now substituting Eqs. (2), (4), (6), and (8) into Eq. (10) and employing the Theorem of minimum potential energy, the following equation is obtained:

$$[K]\{\delta\} - \{F\}_p = 0 \tag{11}$$

where the stiffness matrix $[K]$ and the nodal force vector $\{F\}_p$, due to the surface forces, are calculated as follows:

$$\begin{aligned}[K] &= \int_v [B]^T[\bar{Q}][B]\, dv \\ &= \int_v \{[B_{11}]^T, [B_{31}]^T, \ldots, [B_{r1}]^T, \ldots, [B_{mn}]^T, \ldots, [B_{rr}]^T\}[\bar{Q}] \\ &\times \{[B_{11}], [B_{31}], \ldots, [B_{r1}], \ldots, [B_{mn}], \ldots, [B_{rr}]\}\, dv \end{aligned} \tag{12}$$

$$\begin{aligned}\{F\}_p &= \int_s [N_d]^T[N_p]\{p_0\}\, ds \\ &= \int_s \{[N_{d11}]^T, [N_{d31}]^T, \ldots, [N_{dr1}]^T, \ldots, [N_{dmn}]^T, \ldots, \\ &\times [N_{drr}]^T\}\{[N_{d11}], [N_{d31}], \ldots, [N_{dr1}], \ldots, [N_{dmn}], \ldots, \\ &\times [N_{drr}]\}\{p_0\}\, ds \end{aligned} \tag{13}$$

Since sine and cosine series are used in the displacement and the surface force loads functions, it is found that due to their orthogonality properties

$$\int_v [B_{mn}]^T[\bar{Q}][B_{m'n'}]\, dv = 0 \qquad (\text{for } mn \neq m'n') \tag{14a}$$

$$\int_s [N_{dmn}]^T[N_{pm'n'}]\, ds = 0 \qquad (\text{for } mn \neq m'n') \tag{14b}$$

Therefore, all the off-diagonal matrices in the calculation of Eqs. (12) and (13) become zero and the entire matrix is uncoupled:

$$[K] = \sum_m^r \sum_n^r [K_{mn}] = \sum_m^r \sum_n^r \int_v [B_{mn}]^T[\bar{Q}][B_{mn}]\, dv \tag{15}$$

$$\{F\}_p = \sum_m^r \sum_n^r [F_{mn}]_p = \sum_m^r \sum_n^r \int_s [N_{dmn}]^T[N_{pmn}]\{p_{0mn}\}\, ds \tag{16}$$

It is now possible to solve the diagonal matrices for every m and n individually.

$$\sum_m^r \sum_n^r ([K_{mn}]\{\delta_{mn}\} - \{F_{mn}\}_p) = 0 \tag{17}$$

Transforming this equilibrium equation for an element to the entire system and summing up over the total cylindrical shell, all equilibrium equations can be solved. Then these solutions are summed up for every m and n. This equilibrium equation in the radial direction is enforced at the ply interfaces and thus the method apparently has a significant advantage over two-dimensional shell theories.

When the thick-walled cylindrical shell is subjected to only axially symmetric loading—that is, an external pressure and/or an internal pressure—an axisymmetric deformation may be considered and the terms of v and $\partial(\ )/\partial\theta$ stated above are eliminated.

Results and Discussion

Convergence

By way of checking the formulation and the computer program, the thick-walled cylindrical isotropic shells ($h/R = 0.2$

Table 1 Comparisons of nondimensional stresses and deflection obtained with two mesh divisions in finite element method

	$h/R = 0.2$		$h/R = 0.5$	
	20 Elem.	10 Elem.	20 Elem.	10 Elem.
σ_z/p_i				
$z/h = 0.0$	−0.965	−0.932	−0.947	−0.899
$z/h = 0.5$	−0.425	−0.479	−0.316	−0.367
$z/h = 1.0$	−0.019	−0.037	−0.011	−0.023
σ_y/p_i				
$z/h = 0.0$	5.003	4.970	2.068	2.018
$z/h = 0.5$	4.464	4.520	1.439	1.440
$z/h = 1.0$	4.060	4.121	1.135	1.147
$wE/p_i h$				
$z/h = 0.0$	24.016	24.021	3.629	3.628
$z/h = 0.5$	22.958	22.962	3.066	3.065
$z/h = 1.0$	22.220	22.224	2.806	2.805

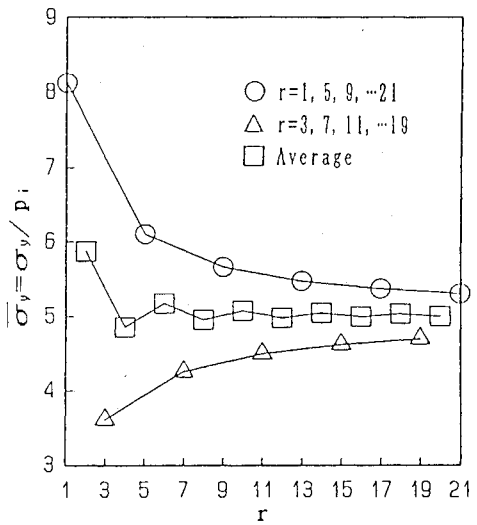

Fig. 2 Circumferential stress in the inner element as a function of number of terms in the series.

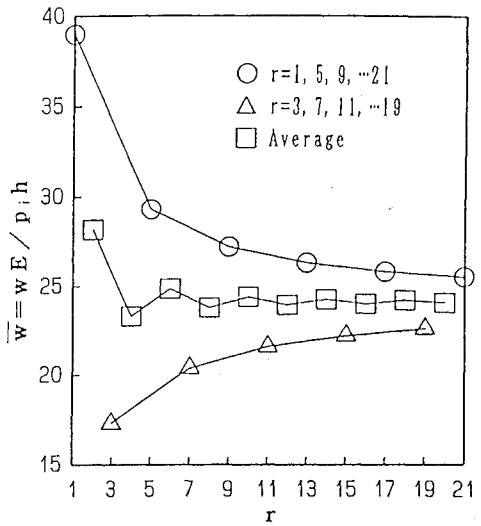

Fig. 3 Lateral deflection on the inner radius as a function of number of terms in the series.

and 0.5), subjected to a uniform internal pressure p_i, have been analyzed by use of 10 and 20 cylindrical elements in the finite element method, respectively.

To discuss the effect of mesh division on the numerical results, nondimensional stresses $\bar{\sigma}_z$ ($= \sigma_z/p_i$), $\bar{\sigma}_y$($= \sigma_y/p_i$) and deflection $\bar{w}$($= wE/p_i h$) at $x = L/2$ and $\theta = \pi/2$ calculated by use of 121 terms (m,n = 1,3,5, ..., 19, 21) in every Fourier series are shown in Table 1. Since the convergance of these values, especially deflection, are given, 20 or 24 cylindrical elements are used in the following results.

In Figs. 2 and 3, $\bar{\sigma}_y$ and $\bar{w}$ are plotted against r, the last number of the Fourier series that is the same for m and n. The overestimated values against the accurate one are obtained for the case of the last wave number of the Fourier series r = 1, 5, 9, ..., 21. On the other hand, the underestimated values are obtained for the case of r = 3, 7, 11, ..., 19. The averages of the last and the next to last results efficiently give the convergent values with fewer terms in the Fourier series. These averaged values are plotted together with the over- and underestimated values. It can be concluded from these figures that the convergent values are obtained when r is taken as 21; namely, the total terms in the Fourier series are taken to be 121. The following numerical results are expressed by use of these averaged values and r = 21.

Comparison with Other Theories

To compare the present results with other approaches, the results of thick-walled cylindrical isotropic shells (h/R = 0.2 and 0.5) with 20 elements in FEM and 121 terms in Fourier series under an internal pressure p_i are used. Since strain components ϵ_x and ϵ_y in the present theory vary linearly in the through-the-thickness direction, stress components σ_x, σ_y, and σ_z are given as the average values over the cylindrical element.

All nondimensional variable quantities, $\bar{\sigma}_y = \sigma_y/p_i$, $\bar{\sigma}_z = \sigma_z/p_i$, and $\bar{w} = wE/p_i h$ are compared with Vinson's[2] and Lamé's solutions in Table 2. For both h/R cases, it is clearly seen that the present theory agrees extremely well with both solutions. The displacements agree within 1%, and the stresses on the inner surface agree within 5% because of taking the average over the element. Hence, the present results are virtually identical with both analytical values.

Laminated Thick-Walled Cylindrical Shells

A laminated thick-walled cylindrical shell of graphite/epoxy (950/6000ST), consisting of $(90°_5/0°_5/90°_5)_8$ layup, is considered here, in which 0 and 90 deg mean that the axis of the unidirectional prepregs are parallel and perpendicular to the x axis of the cylindrical shell, respectively. Each element in the finite element method is considered, as the laminated cylinder consisting of five identical layers and the unidirectional prepregs have the following properties: E_{11} = 104.11 GPa, $E_{22} = E_{33}$ = 9.65 GPa, $G_{12} = G_{13}$ = 4.48 GPa, G_{23} = 3.24 GPa, $\nu_{12} = \nu_{13} = 0.30$, $\nu_{23} = 0.49$. Three stress distributions along the through-the-thickness direction for the shell with an inner radius of 8.89 cm and an outer radius of 10.41 cm loaded by 82.7 MPa external hydrostatic pressure are shown in Figs. 4 and 5. These stresses are normalized by the absolute value of the external pressure p_o.

Table 2 Comparisons among present results: Lamé plain strain solutions and Vinson's results

	h/R = 0.2			h/R = 0.5		
	Vinson	Lamé	Present theory	Vinson	Lamé	Present theory
σ_z/p_i						
z/h = 0.0	−1	−1	−0.965	−1	−1	−0.947
z/h = 0.5	−0.425	−0.425	−0.425	−0.316	−0.316	−0.316
z/h = 1.0	0	0	−0.019	0	0	−0.011
σ_y/p_i						
z/h = 0.0	5.03	5.05	5.01	2.06	2.13	2.07
z/h = 0.5	4.49	4.48	4.47	1.45	1.44	1.44
z/h = 1.0	4.04	4.05	4.06	1.10	1.13	1.14
$wE/p_i h$						
z/h = 0.0	24.0	24.1	24.0	3.62	3.64	3.63
z/h = 0.5	23.2	23.1	23.0	3.05	3.08	3.09
z/h = 1.0	22.3	22.3	22.2	2.80	2.82	2.81

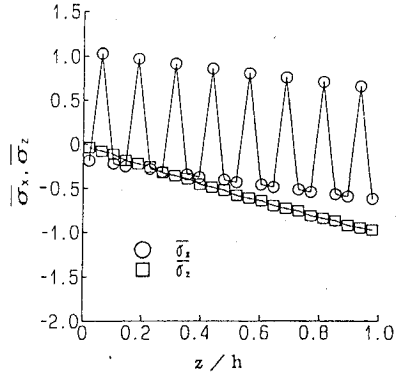

Fig. 4 Nondimensional stress distributions in the through-the-thickness direction.

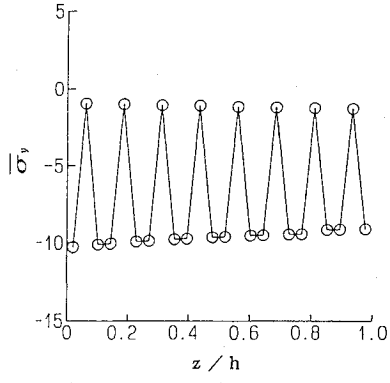

Fig. 5 Nondimensional stress distributions in the through-the-thickness direction.

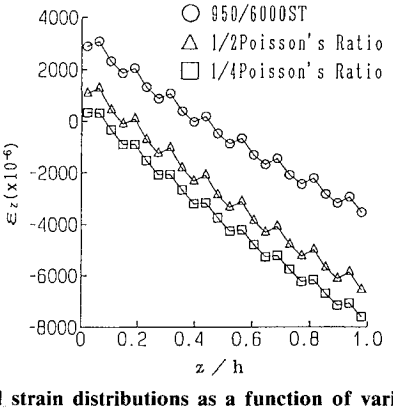

Fig. 6 Radial strain distributions as a function of various Poisson ratios.

Although $\overline{\sigma_x}$ in 90- and 0-deg layers show compressive and tensile stresses, respectively, their summation in the through-the-thickness direction becomes zero, indicating no resultant force in the axial direction. The maximum compressive circumferential stress $\overline{\sigma_y}$ occurs in the 90-deg layer adjacent to the inner surface, and its value is almost ten times that of the external pressure. Since this stress is compressive along the direction of fibers and is more than 850 MPa, there is a risk of a compressive failure, for example, fiber kinking in 90-deg layers closest to the inner surface. On the other hand, the radial stress $\overline{\sigma_z}$ is supposed to change continuously from 0 on the inner surface to 1 on the outer surface.

Next, the radial strain distribution ϵ_z along the through-the-thickness direction is shown in Fig. 6. The maximum tensile strain, 3380μ, occurs in the 0-deg layer closest to the inner surface because of the compressive stress σ_y and comparatively larger Poisson's ratio ν_{23}. This tensile strain decreases rapidly to a compressive one at the outer surface. Since the tensile strain causes delamination in the through-the-thickness direction, common design practice for the laminated composite structures will avoid high tensile loading and straining of the laminate in the through-the-thickness direction.

To examine the effect of Poisson's ratios on ϵ_z, two cases are studied, in which all material properties are held constant, except that the Poisson's ratio are reduced to one-half and one-quarter of the original values. The results are also given in Fig. 6, together with the original case. The magnitude and the range of tensile ϵ_z in both cases become smaller than in the original case, even though $\overline{\sigma_z}$ and $\overline{\sigma_y}$ values hardly change.

This suggests that improved material design for lower Poisson's ratios in composite materials is one of the means to prevent the delamination in laminated thick-walled cylindrical shells subjected to high external pressure loads.

Conclusions

A finite cylindrical element method requiring a thick-walled cylindrical shell to be divided into a number of thin cylindrical shell elements in the through-the-thickness direction is formulated for obtaining stresses and deformation in laminated thick-walled cylindrical anisotropic shells. The main features of this approach, obtained through several numerical calculations, can be summarized as follows:

1) The present method is simple but accurate, and requires small computer storage and little data input in the case of a thick-walled cross-ply cylindrical graphite/epoxy shell.

2) When the thick-walled cylindrical shell laminated with graphite/epoxy (950/6000ST) consisting of a $(90°_5/0°_5/90°_5)_8$ layup is subjected to an external hydrostatic pressure, the significant tensile radial strain occurs in 0-deg layers closest to the inner surface, and causes an interlaminar failure of the laminated thick-walled cylindrical shell. Furthermore, there is a risk of a compressive failure along the direction of fibers, for example, fiber kinking in 90-deg layers closest to the inner surface.

3) One useful approach in reducing this tensile strain, as made clear by numerical calculations, is the use of proper material design to reduce Poisson's ratios in composite material systems.

The effects of thermal residual stresses, the laminate angle, and/or the constitution of the layup in composite material systems on the design for the laminated thick-walled cylindrical anisotropic shell is being studied at this time and will be reported on shortly.

Acknowledgment

This work was primarily performed during the period when the primary author was a visiting professor at the University of Delaware. The author wishes to thank members of Nihon University and the University of Delaware who made this sabbatical possible.

References

[1]Comings, E. W., *High Pressure Technology,* McGraw-Hill, New York, 1956.

[2]Vinson, J. R., "Methods of Analysis for Very Thick-Walled Cylindrical Shells," *Transactions of the ASME, Journal of Engineering for Industry,* Feb. 1975, pp. 175-181.

[3]Hyer, M. W., "Hydrostatic Response of Thick Laminated Composite Cylinders," *Journal of Reinforced Plastics and Composites,* Vol. 7, 1988, pp. 321-340.

[4]Hyer, M. W., and Cooper, D. E., "Stresses and Deformations in Composite Tubes Due to a Circumferential Temperature Gradient," *Transactions of the ASME, Journal of Applied Mechanics,* Vol. 53, No. 4, 1986, pp. 757-764.

[5]Hyer, M. W., Cooper, D. E., and Cohen, D. "Stresses and Deformations in Cross-Ply Composite Tubes Subjected to a Uniform Temperature Change," *Journal of Thermal Stresses,* Vol. 9, 1986, pp. 97-117.

[6]Peros, V., "Thick-Walled Composite Material Pressure Hulls: Three-Dimensional Laminate Analysis Considerations," M.S. Thesis, Univ. of Delaware, Newark, DE, Dec. 1987.

[7]Vanderpool, M. E., and Bert, C. W., "Vibration of a Materially, Monoclinic, Thick-Wall Circular Cylindrical Shell," *AIAA Journal,* Vol. 19, No. 5, 1981, pp. 634-641.